Lower-Stratospheric and Upper-Tropospheric Disturbances Observed by Radiosondes over Thailand during January 2000

SHIN-YA OGINO

Institute of Observational Research for Global Change, Japan Agency for Marine-Earth Science and Technology, Yokosuka, Japan

KAORU SATO

Department of Earth and Planetary Science, Graduate School of Science, The University of Tokyo, Tokyo, Japan

MANABU D. YAMANAKA

Institute of Observational Research for Global Change, Japan Agency for Marine-Earth Science and Technology, Yokosuka, and Graduate School of Science and Technology, Kobe University, Kobe, Japan

AKIRA WATANABE

Cluster of Science and Technology, Fukushima University, Fukushima, Japan

(Manuscript received 26 January 2004, in final form 28 February 2006)

ABSTRACT

Lower-stratospheric and upper-tropospheric disturbances over Thailand during 12–21 January 2000 were studied using the Global Energy and Water Cycle Experiment (GEWEX) Asian Monsoon Experiment-Tropics (GAME-T) intensive rawinsonde observations with fine temporal sampling intervals of 3 h. Analysis was focused on the wind disturbances with a period shorter than about 10 days. Frequency spectra showed three distinct peaks: a 1-day period above a height of 20 km, a near-inertial period around 19 and 27 km, and periods of 2.5–9 days (or longer) in the height range of 12–17 km.

The wave with a 1-day period was interpreted as a diurnal tide. A comparison with the migrating tide in the global-scale wave model showed that the observational results had larger amplitude and shorter vertical wavelength than the model. The difference between the observation and the model may be caused by the superposition of the nonmigrating tide.

The wave with the near-inertial period was interpreted as an internal inertial gravity wave. A hodograph analysis was performed in order to investigate the wave properties. It was found that the wave, which appeared at a height around 19 km (just above the tropopause level), propagated southwestward with a ground-based group velocity of about 1.4 m s^{-1}.

The longer period disturbances, which appeared at heights of 12–17 km, had layered structures with the vertical scales of 2–4 km. They were considered to be due to inertial instability, based on the fact that the potential vorticity of the background atmosphere was nearly zero and that their phase structures were consistent with theory. It was shown by a backward trajectory analysis that the air parcel with negative potential vorticity had its origin in equatorial Indonesia. It was also shown by a forward trajectory analysis that the air parcel was transported to the Pacific south of Japan. This is consistent with the existence of similar layered disturbances that are shown using rawinsonde data at a station there.

1. Introduction

Gravity waves are important because they play an essential role in maintaining the mean structure of the earth's atmosphere by transporting momentum from sources to sinks. Therefore, the global distribution of momentum flux associated with gravity waves must be known in order to quantitatively understand global circulation. So far, many authors have tried to describe the global features of gravity waves. Meridional distributions of wave amplitude have been studied by many researchers (Hirota 1984; Kitamura and Hirota 1989; Eckermann et al. 1995; Allen and Vincent 1995; Ogino et al. 1995, 1997, 1999a,b; Sato et al. 1999, 2003;

Corresponding author address: Shin-Ya Ogino, Institute of Observational Research for Global Change, Japan Agency for Marine-Earth Science and Technology, 2-15, Natsushima-cho, Yokosuka 236-0061, Japan.
E-mail: ogino-sy@jamstec.go.jp

Yamamori and Sato 2006). Most of these authors studied not only the meridional variation, but also altitudinal or seasonal variations, or both, of gravity waves.

They clarified many important features of gravity wave distribution. However, there have been many uncertainties regarding the global distribution of gravity waves. Recently, satellite observations have revealed the global distributions of gravity wave amplitude (Fetzer and Gille 1994, 1996; Wu and Waters 1996a,b; Tsuda et al. 2000). However, because these studies were based on temperature data only, wave properties such as wave frequency and propagation direction were not studied, and therefore, the momentum transport by gravity waves could not be quantified. Therefore, it is still important to describe the wave characteristics at various locations, especially at places where no observational work has been conducted. Southeast Asia is one of the most important regions that has not been studied. This paper reports worthwhile results of the description of the wave characteristics at NongKhai (18°N, 103°E), Thailand, on the Indochina Peninsula in Southeast Asia during 12–21 January 2000.

Descriptions about the rawinsonde observations and data are given in section 2. In section 3, frequency spectra are calculated and the existence of the three types of disturbances is shown. In section 4, the three types of disturbances are interpreted as a diurnal tide, internal inertial gravity waves, and disturbances due to inertial instability. Section 5 summarizes the results and discusses the meaning of this work.

2. Observation and data

Six enhanced rawinsonde observation campaigns were conducted by the Global Energy and Water Cycle Experiment (GEWEX) Asian Monsoon Experiment-Tropics (GAME-T) project from 1996 to 2000 in Thailand and neighboring countries. Four of the six enhanced observation campaigns were conducted in the rainy season, while the remaining two were conducted in the dry season. Observation periods of the enhanced observation campaigns were either about 2 or 4 weeks. During each campaign period, rawinsondes were launched 8 or 4 times a day (every 3 or 6 h) using the Atmospheric Instrumentation Research, Inc. (AIR) radiosonde system.

In this paper, the results obtained from the data in the sixth campaign are described. The sixth campaign was conducted for about 10 days during 12–21 January 2000 at NongKhai (18°N, 103°E), which is located in the northeastern part of Thailand and in the central part of the Indochina Peninsula (Fig. 1). During this campaign

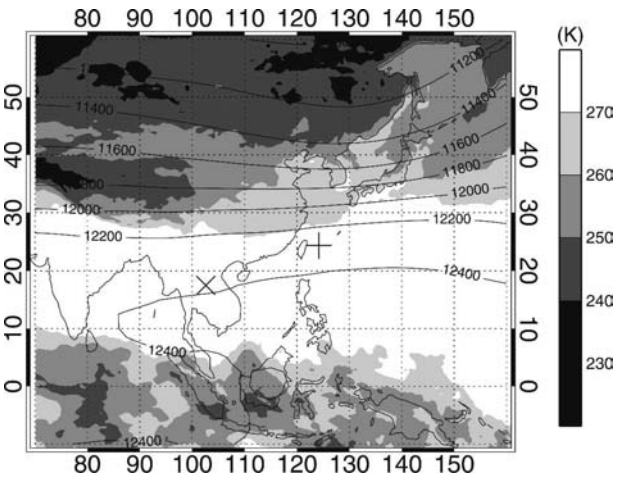

FIG. 1. A cross and plus sign denote the locations of NongKhai (18°N, 103°E) and Ishigakijima (24°N, 124°E), respectively. Contours show the NCEP geopotential height at 200 hPa and shades show the GMS blackbody temperature. Both are the mean values for the whole observation period of 12–21 January 2000.

period, rawinsondes were launched every 3 hours continuously for about 10 days (Fig. 1). In this campaign, the data in the lower stratosphere and upper troposphere were the most continuously obtained in time and height among the six campaigns because balloons with high resistance to a low-temperature condition were used so that the balloons would not burst near the tropopause height. This continuous and high-resolution data exhibits clear wavy structures in the lower stratosphere and layered structures in the upper troposphere.

The original sampling interval in each sounding was 10 s, which corresponds to a height interval of about 50 m. The data obtained were linearly interpolated into 50-m height intervals.

Additionally, the 6-hourly National Centers for Environmental Prediction (NCEP) reanalysis data and the Geostationary Meteorological Satellite (GMS) blackbody temperature data were used for describing background fields in relation to excitation sources of gravity waves in section 4b. The 6-hourly NCEP reanalysis data were also used for the calculation of the potential vorticity (PV) and for the backward trajectory analysis in section 4c. The twice-daily operational rawinsonde data at Ishigakijima, Japan (24°N, 124°E), which is one of the most southern rawinsonde stations of the Japan Meteorological Agency (JMA), were also used to describe the layered disturbances over the Pacific Ocean south of Japan.

Figure 2 shows a time–height section of the meridional wind obtained at NongKhai during the sixth enhanced observation period. Clear wave structures are found without any filtering procedure above and near

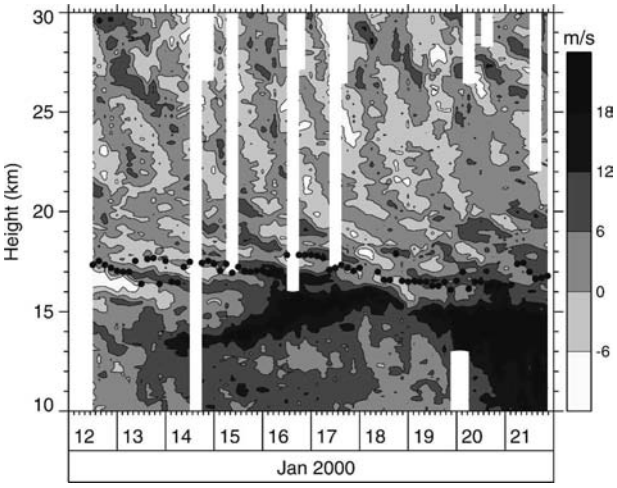

FIG. 2. Time–height section of the meridional wind obtained in the enhanced rawinsonde observation campaign conducted from 12 to 22 January 2000 at NongKhai (18°N, 103°E). Closed circles indicate the cold point tropopause.

the tropopause, indicated by closed circles. These waves show a downward phase progression, which suggests that they are internal waves and are energetically propagating upward. The waves seem to have different structures below and above a height of about 20 km. The waves above about 20 km have longer vertical wavelengths and faster downward phase velocities than the ones below this height. It will be shown in the next section that the waves above 20 km have a 1-day period and those below 20 km have a period near the inertial period (~39 h at the latitude of 18°N).

Layered structures are seen in the upper troposphere (around 15 km) during the time period of 14–21 January. This type of disturbance will be investigated in section 4c. The peak height of meridional wind was moving upward during 14–18 January and downward during 19–21 January. The former and latter period correspond to the passages of synoptic-scale high and low pressure systems, respectively.

Figure 3 shows mean vertical profiles of the zonal and meridional winds averaged over the whole observation period. The westerly wind, more than 10 m s^{-1}, prevails in a height range of 4–14 km with a maximum speed of about 17 m s^{-1} at about 7 km. The southerly wind peaks at about 15 km. It will be shown in section 4c that this southerly wind brings air parcels with (near) negative potential vorticity from the equatorial region. Both zonal and meridional winds become almost zero near the height of 20 km. Above this height, the zonal wind changes to easterly, whereas the meridional wind remains almost zero.

In Fig. 1, the NCEP geopotential height at 200 hPa and the GMS blackbody temperature averaged for the

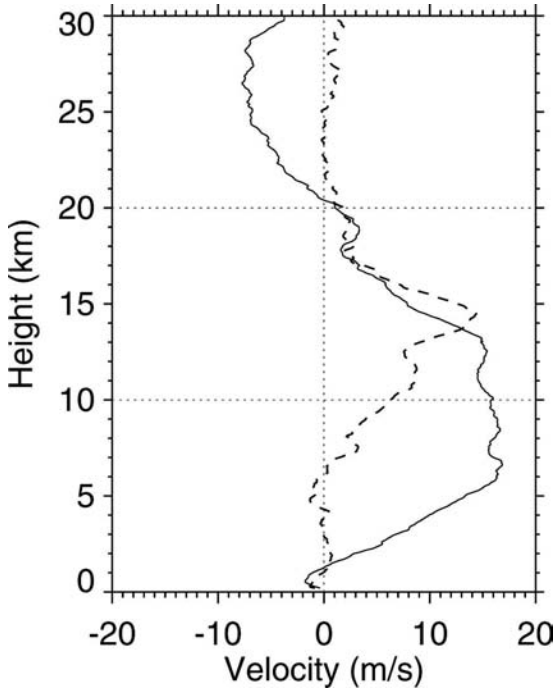

FIG. 3. Mean vertical profiles of the zonal (solid line) and meridional (dashed line) winds averaged over the observation period.

whole observation period are shown. It is seen that the westerly jet stream is located in the latitudes 30°–40°N. In the equatorial region, it is found that active convection occurred during the campaign period.

3. Frequency spectra

The rawinsondes were launched every 3 hours, as mentioned above. Therefore, it is enough to detect the disturbances with a temporal scale of one-half day or longer. Frequency spectral analyses were conducted by utilizing such high-resolution data.

The spectra were calculated using the fast Fourier transform method. Missing data were linearly interpolated in time at each height before the FFT calculation.

Figure 4 shows the height variation of the frequency spectra of meridional wind. In the height range of 20–30 km, spectral peaks with a 1-day period are clearly found. On the other hand, in the height ranges of 18–20 km and 26–28 km, relatively large spectral powers are observed near the inertial period (about 39 h at this latitude). In the height range of 12–17 km, spectral components with longer period (2.5–9 days or longer) are found to have a large power.

The existence of spectral peaks near the inertial period is the same characteristic found by Sato et al. (1999) in the high-resolution, general circulation model

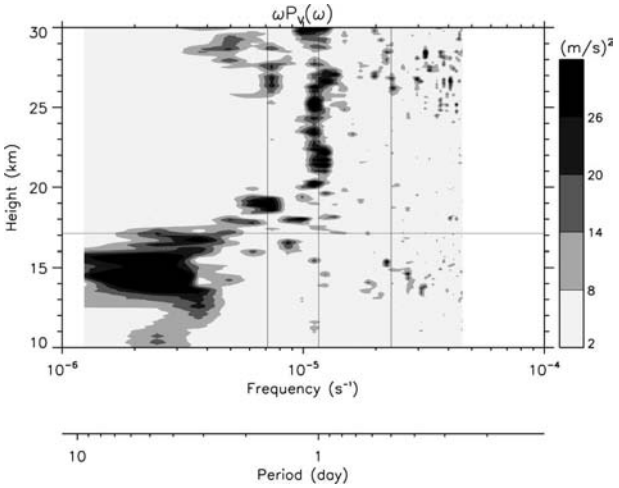

FIG. 4. Height variation of the frequency spectra for meridional wind. The vertical lines indicate, from left to right, the inertial period at NongKhai (about 39 h), 1 day, and a half day. The horizontal line indicates the mean tropopause height during the observation period.

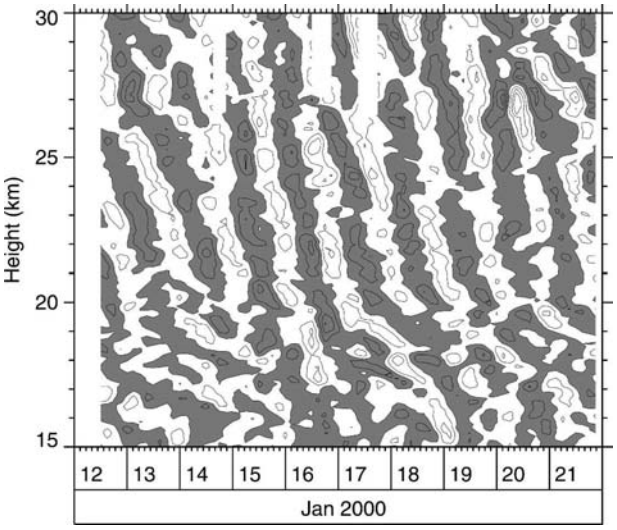

FIG. 5. Time–height section of the 1-day component of meridional wind. The 1-day components were extracted by a bandpass filter in time with cutoff lengths of 12 and 36 h. The contour interval is 2.5 m s^{-1}; regions with positive values are shaded.

(GCM) experiment. They found that the frequency spectra in the lower stratosphere have distinct peaks near the inertial period as a common characteristic through wide latitude ranges. Although such a characteristic is found only in a limited height range in the present case, it is noteworthy that the characteristic is confirmed by real observational data at this latitude, where temporal high-resolution data has not been collected.

4. Interpretation

a. One-day waves: Migrating and nonmigrating tides

The 1-day components were extracted by a bandpass filter in time with cutoff lengths of 12 and 36 h. The time–height section of the 1-day components of meridional wind is shown in Fig. 5. Clear wave structures are found in the height range of 20–30 km.

By fitting each time series at each height to a sinusoidal curve with the period of 1 day, the phase and amplitude of the 1-day wave were estimated. The result is shown by the dotted lines in Fig. 6. It is found that, above about 20 km, the amplitude abruptly increases and the phase possesses a characteristic of downward progression with time. The vertical wavelength of the wave estimated from this figure is about 12 km. In Fig. 6, the amplitude and phase of the migrating tide, which appeared in the Global Scale Wave Model (GSWM) by Hagan et al. (1999), are also plotted as solid lines with plus signs. Generally speaking, the observational results and the model agree well. It is noteworthy that the NongKhai station, at 18°N, is where the diurnal tidal amplitude of meridional wind is maximized (Hagan et al. 1999).

However, we find some differences between the observation and the model, which seem to have physical meaning. For the amplitude in the lower stratosphere, the observational results are greater than the model. For the phase, the observational results have slower downward progression than the model, which means that the vertical wavelength of the observation (about 12 km) is shorter than that of the model (about 25 km). Smaller amplitudes and shorter vertical wavelengths than the model have been shown by previous observational studies (e.g., Fukao et al. 1980; Tsuda et al. 1994a), although the observational results consistent with theory have been also shown (e.g., Hitchman and Leovy 1985). In the real atmosphere, the nonmigrating tide, which does not move with the sun, is also excited and propagating, while the GSWM does not express this type of wave. It is suggested that the nonmigrating tide has a shorter vertical wavelength than the migrating tide (e.g., Tsuda and Kato 1989). Therefore, the larger amplitude and shorter vertical wavelength in observations than in the model, which includes only migrating tides, are reasonable if the observational results come from the superposition of the migrating and nonmigrating tides.

b. Near-inertial period waves: Inertial gravity waves propagating toward the equator

1) WAVE STRUCTURES

The waves with the near-inertial period were extracted by a bandpass filter in time with cutoff lengths

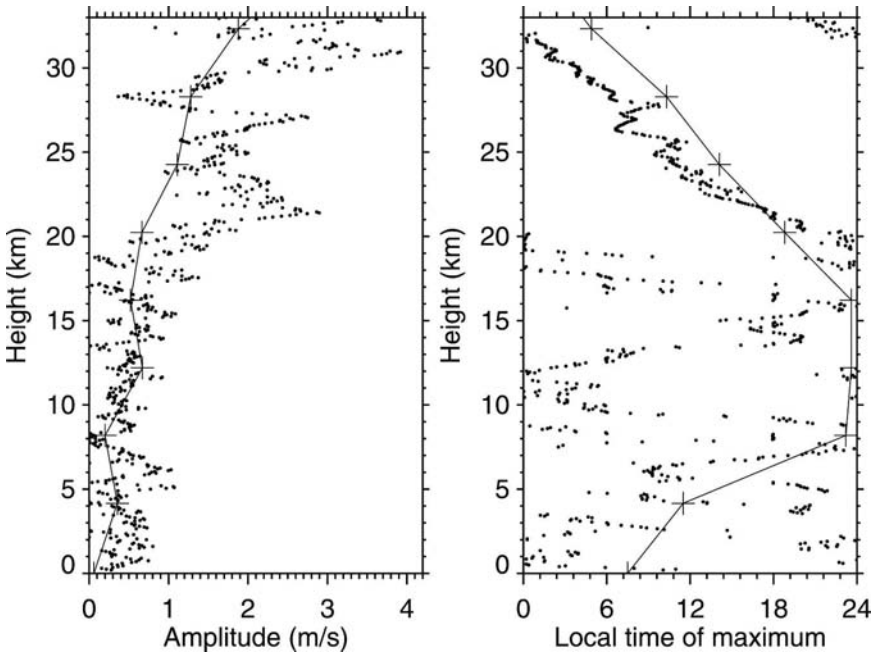

FIG. 6. Vertical profiles of (left) amplitude and (right) phase for the 1-day wave. Dotted lines indicate the results obtained from observation; solid lines with plus signs indicate the results in the GSWM by Hagan et al. (1999).

of 30 and 69 h. The meridional wind variation extracted by this filtering is shown in Fig. 7. Corresponding to the spectral peaks shown in Fig. 4, waves with vertical scales of 1–1.5 km around the 18-km height and those with vertical scales of 2–4 km around the 27-km height are found. The wave properties were examined by analyzing hodographs (e.g., Sato 1994; Sato et al. 2003). The result obtained from the wave around 18 km is shown below. Meaningful wave parameters could not be analyzed for the waves around 27 km in height, probably because they are a mixture of other types of disturbances. Therefore, they are not discussed further in this paper.

An example of the hodographs for the waves around 18 km is shown in Fig. 8. The hodograph is drawn with the horizontal winds in the height range of 17.50–18.45 km at 1200 UTC 17 January 2000 (Fig. 8). Additional bandpass filtering in height with cutoff lengths of 0.5 and 3.0 km was applied before performing the hodograph analysis in order to extract a monochromatic structure more clearly. A clear elliptic rotation of the horizontal wind vector is found in Fig. 8. Since the shape of the hodograph ellipse did not greatly change for several days, it is thought that the waves have the same origin and the same propagation path during the observation period. The wind vector rotates clockwise with height, which indicates upward energy propagation of the wave.

The vertical wavelength was estimated directly from the height difference of one elliptic cycle of the hodograph. The direction of the horizontal wavenumber vector was determined from the orientation of the ellipse and the phase relationship between the wind and

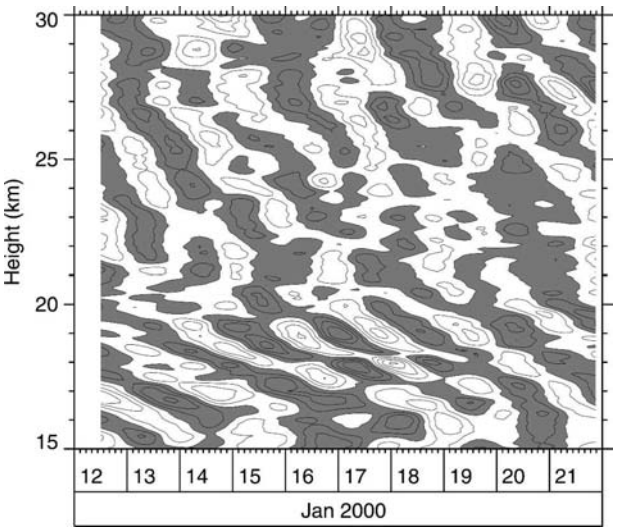

FIG. 7. Time–height section of the near-inertial period components of meridional wind. The components were extracted by a bandpass filter in time with cutoff lengths of 30 and 69 h. The contour interval is 1.5 m s^{-1}; regions with positive values are shaded.

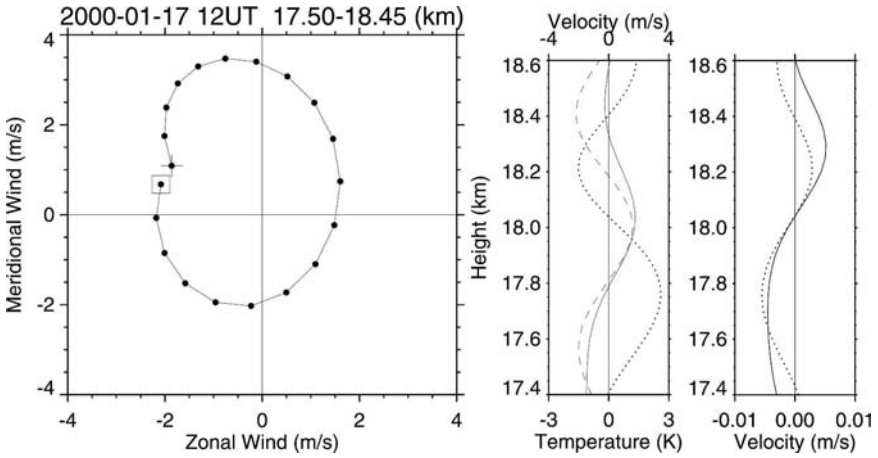

FIG. 8. (left) A hodograph drawn with the horizontal winds in the height range of 17.50–18.45 km at 1200 UTC 17 Jan 2000. Plus signs and squares indicate the bottom and top points of the height range. (middle) Corresponding vertical profiles of temperature (solid line), meridional wind (dotted line), and zonal wind (dashed line). Bandpass filters in time with cutoff lengths of 30 and 69 h and in height with cutoff lengths of 0.5 and 3 km were applied to the data plotted in the panels in order to extract a monochromatic wave. (right) Vertical profiles of vertical wind derived from the thermodynamic equation (solid line) and from the continuity equation (dotted line).

temperature fluctuations, as shown in the right panel of Fig. 8. The intrinsic wave frequency $\hat{\omega}$ was estimated from the ratio of the parallel to perpendicular amplitudes of the horizontal winds to the horizontal wavenumber vector, which corresponds to the ratio of long ($|U|$) to short ($|V|$) axes of the ellipse:

$$|\hat{\omega}| = \frac{|U|}{|V|}|f|,$$

where f is the inertial frequency. The horizontal wavenumber $\mathbf{k}$ was calculated by using the dispersion relationship of a hydrostatic inertial gravity wave:

$$|\mathbf{k}|^2 = \frac{\hat{\omega}^2 - f^2}{N^2} m^2,$$

where N is the Brunt–Väisälä frequency and m is the vertical wavenumber. The wave parameters estimated by analyzing the hodograph shown above are listed as follows:

- Vertical wavelength $2\pi/|m| \approx 1.0$ km
- Direction of horizontal wavenumber vector $\mathbf{k} \approx 180°$ (southward)
- Intrinsic wave period $2\pi/|\hat{\omega}| \approx 28$ h
- Horizontal wavelength $2\pi/|\mathbf{k}| \approx 630$ km
- Intrinsic horizontal phase velocity $\hat{\omega}/|\mathbf{k}| \approx 6.2$ m s^{-1} (southward)

The ground-based wave frequency ω was estimated by applying $\hat{\omega}\mathbf{k}$ obtained from the hodograph analysis into the Doppler relationship equation:

$$\hat{\omega} = \omega - \mathbf{k} \cdot \bar{\mathbf{u}},$$

where $\bar{\mathbf{u}}$ is the background horizontal wind, which was calculated in this case by averaging the horizontal winds in the height range 17.50–18.45 km during the period from 1200 UTC 16 January 2000 to 1200 UTC 18 January 2000. The ground-based wave period $2\pi/\omega$ was estimated as ~39 h, consistent with the frequency spectral peak near the inertial period (~39 h) shown in section 3. This suggests that the results of the hodograph analysis are reliable.

The vertical wind component w' can be derived from two methods: one utilizes the thermodynamic equation

$$w' = i\frac{\hat{\omega}}{\partial\bar{T}/\partial z + g/c_p} T',$$

where $\bar{T}$ is the background temperature, g is the gravity acceleration, c_p is the specific heat of dry air at constant pressure, and T' is the temperature component; and another utilizes the continuity equation

$$w' = -\frac{|\mathbf{k}|}{|m|} v',$$

where v' is the meridional wind component and we assume that the gravity wave propagates southward. Vertical profiles of w' derived from the two methods are shown in Fig. 8. The two profiles agree well in both amplitude and phase except for a part of the upper height range, which indicates that the wave analyzed here can be well described by the linear theory of gravity waves and that the analyses in this section are reli-

able. By using w' derived from the thermodynamic equation, the upward flux of northward momentum $\overline{v'w'}$ associated with the gravity wave analyzed here is estimated as 6.0×10^{-3} m^2 s^{-2}. Note that, since the wave propagated southward, $\overline{u'v'}$ and $\overline{u'w'}$ are theoretically expected to be zero. The $\overline{v'w'}$ estimated above is comparable to the result ($\approx 10^{-3}$ m^2 s^{-2}) in the subtropical lower stratosphere in the GCM experiment by Sato et al. (1999). From the gravity wave parameters observed in the subtropics using the meridional scan experiment by Sato et al. (2003), the upward flux of poleward momentum is estimated as one order larger than our result. Some observational studies for midlatitude gravity waves (e.g., Sato 1994; Vincent et al. 1997) also showed larger values (10^{-1}–10^{-2} m^2 s^{-2}). It must be noted that the wind fluctuations with short vertical wavelengths shown in this study were possibly attenuated by the smoothing procedure in the wind measurement of radiosonde observation (see, e.g., Yamanaka et al. 1996; Ogino et al. 1999b).

2) EXCITATION SOURCE

The ground-based group velocity

$$\frac{N^2}{\hat{\omega}m^2}\mathbf{k} + \bar{\mathbf{u}}$$

was estimated as ~2.5 m s^{-1} toward the southwest (~120° measured clockwise from the north), that is, from the midlatitudes toward the equatorial region. The strong midlatitude jet stream or related disturbances are possible candidates for the excitation source of the gravity waves, as suggested by many authors (e.g., Hirota and Niki 1985; Kitamura and Hirota 1989). Sato (1994) showed equatorward propagation of gravity waves around the jet stream axis in northern winter. This is consistent with the southward propagation of the gravity wave analyzed here. Indeed, the westerly jet stream and the related convective activities were located in the midlatitude region as shown in Fig. 1. However, in order to identify the excitation source of the wave, an advanced analysis using a ray-tracing method, for example, is needed.

Cumulonimbus convection in the equatorial region, as seen in Fig. 1, is one of the possible candidates for an excitation source of gravity waves (Tsuda et al. 1994b; Shimizu and Tsuda 1997), and it is expected that the gravity waves excited near the equator may propagate poleward (Sato et al. 1999). However, at least during the enhanced observation period in January 2000, we did not observe such poleward (northward) propagating gravity waves.

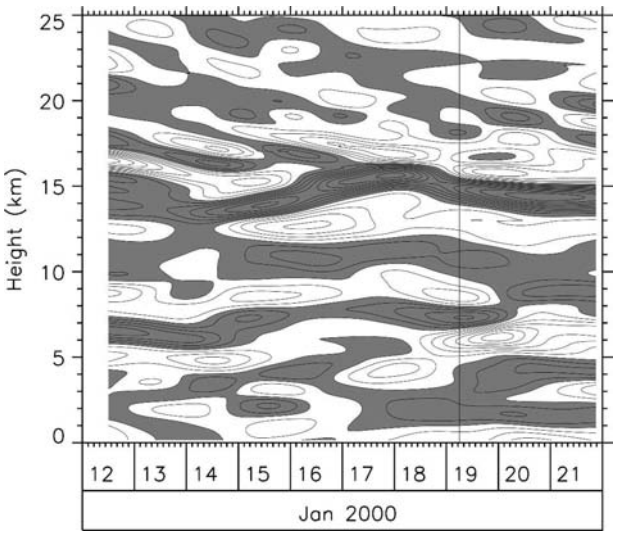

FIG. 9. Time–height section of the meridional wind at Nong-Khai. A low-pass filter in time with a cutoff length of 2 days and a bandpass filter in height with cutoff lengths of 1.5 and 6 km were applied to the original data. Dark shaded regions denote positive values and light shaded negative; contour intervals are 1 m s^{-1}. A vertical line indicates 0600 UTC 19 Jan 2000.

c. *Disturbances due to inertial instability*

The frequency spectra of meridional wind (Fig. 4) shows the existence of relatively long period disturbances (2.5–9 days, or longer) in the height region near and below the tropopause (12–17 km). In this section, these layered disturbances are analyzed in terms of inertial instability.

To extract long period disturbances, a low-pass filter in time with a cutoff length of 2 days was applied to the original time series. Since the layered structures with a vertical scale of 2–4 km dominated after the low-pass filtering, in order to extract them more clearly a bandpass filter in height with cutoff lengths of 1.5 and 6 km was also applied. The result is shown in Fig. 9. Layered structures are found in a height range near and below the tropopause level (12–17 km) during almost the entire observation period.

Sato and Dunkerton (2002) showed the frequent appearance of layered structures south of Japan over the western Pacific in the northern wintertime. They showed that the disturbances are likely due to inertial instability based on evidence that the background potential vorticity is nearly zero or frequently negative, that the meridional and zonal wind perturbation has negative correlation, and that the meridional wind perturbation has larger amplitude than the zonal wind.

They also showed that the inertially unstable air parcels traced back to the equatorial region, passing through the Indochina Peninsula. Therefore, there is a

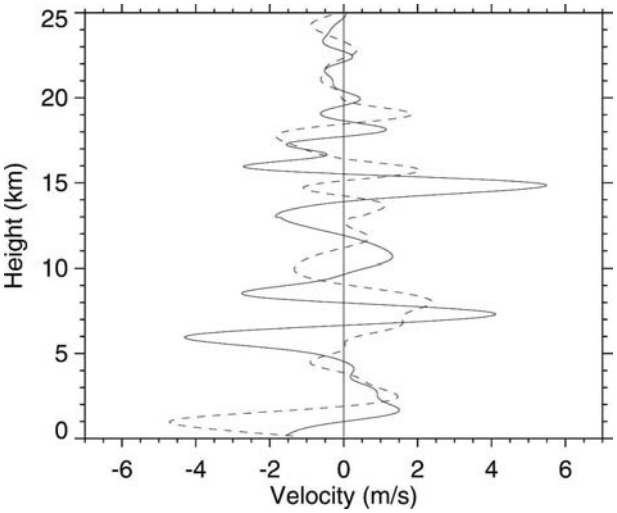

FIG. 10. Vertical profiles of meridional (solid line) and zonal (dashed line) wind components at NongKhai at 0600 UTC 19 Jan 2000.

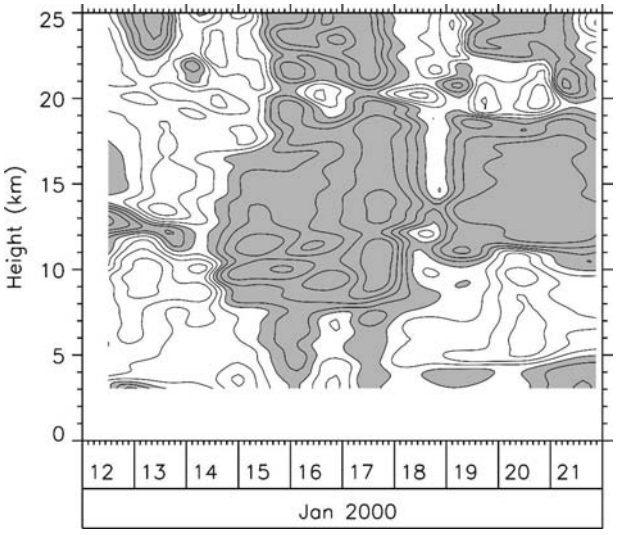

FIG. 11. Time–height section of correlation coefficients between the meridional and zonal wind perturbations with the temporal scale longer than 2 days and vertical scale of 1.5–6.0 km. A correlation coefficient was calculated at each height and each time using the data in a height range 3 km below and 3 km above the height. Shaded regions denote negative correlations; contour intervals are 0.2.

possibility that the disturbances due to inertial instability also occur over the Indochina Peninsula. Here, we examine if the disturbances with a period longer than 2 days observed in the upper troposphere at NongKhai were due to inertial instability.

Figure 10 shows the vertical profiles of the bandpass-filtered meridional and zonal winds at 0600 UTC 19 January 2000, which is indicated by the vertical line in Fig. 9. It is found that the phase relationship between the meridional and zonal winds is almost opposite around 15 km in height. This feature is consistent with the disturbances due to inertial instability. It is also found that the perturbation amplitude of the meridional wind is larger than that of the zonal wind. This is also consistent with disturbances due to inertial instability in the zonally rotating earth's atmosphere. The similar phase relation and amplitude ratio are seen during almost the whole observation period in the upper troposphere as shown, in Figs. 11 and 12.

Figure 13 shows the horizontal distribution of potential vorticity at 0600 UTC 19 January 2000 on the 350-K isentropic surface, which corresponds to about 14-km height at NongKhai. It is found from Fig. 13 that the background PV is nearly zero or negative near NongKhai. Therefore, based on the aforementioned facts, it is highly expected that the layered disturbances are due to inertial instability.

A backward trajectory analysis on the 350-K isentropic surface was performed in order to examine the origin of the air parcel with (near) negative PV in which the layered disturbances were embedded. Such an air parcel must be transported from the Southern Hemisphere since the negative PV cannot be produced in the Northern Hemisphere. The trajectory was calculated by integrating the NCEP reanalysis wind data with a fourth-order Runge–Kutta scheme, which is the same method performed by Sato and Dunkerton (2002). Fig-

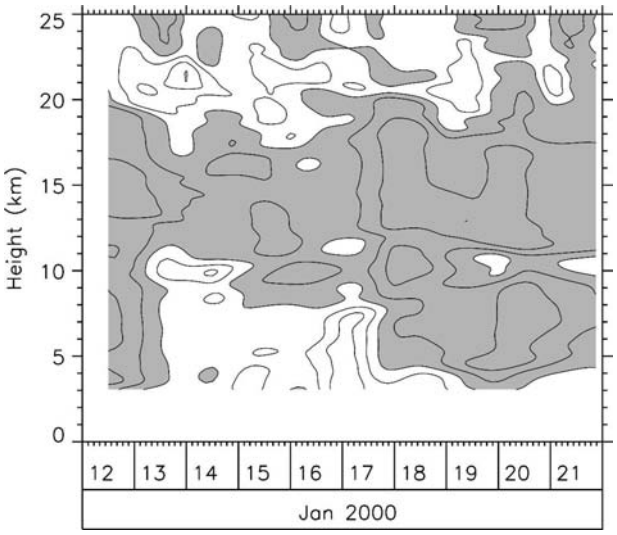

FIG. 12. Time–height section of amplitude ratio between the meridional ($|v'|$) and zonal ($|u'|$) wind perturbations with the temporal scale longer than 2 days and vertical scale of 1.5–6.0 km. Here the amplitude ratio is defined as $(|v'| - |u'|)/(|v'| + |u'|)$, which shows a positive value if $|v'| > |u'|$. The amplitude ratio was calculated at each height and each time using the data in a height range 3 km below and 3 km above the height. Shaded regions denote positive values; contour intervals are 0.2.

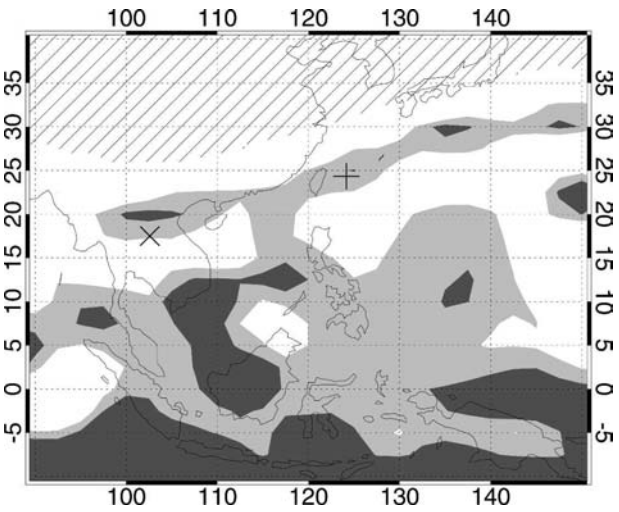

FIG. 13. Horizontal distribution of PV on the 350-K isentropic surface at 0600 UTC 19 Jan 2000. Regions in which PV < 0 (0.1) PVU is dark (light) shaded; stratospheric regions (PV > 1.6 PVU) are hatched. The cross and plus sign denote the locations of NongKhai and Ishigakijima, respectively.

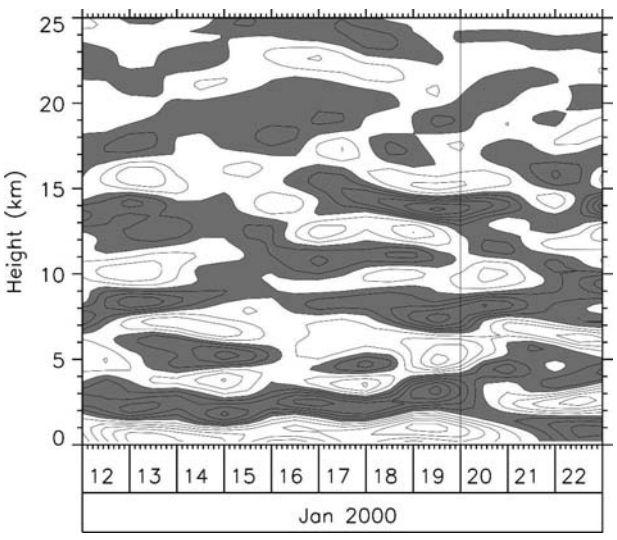

FIG. 15. As in Fig. 9 but for Ishigakijima. The vertical line indicates 0000 UTC 20 Jan 2000.

ure 14 shows a backward trajectory for 5 days starting at NongKhai at 0600 UTC 19 January 2000. It is found that the air was transported from the equatorial Indonesian region within 5 days. This feature is similar to that reported by Sato and Dunkerton for the disturbances due to inertial instability.

Next, disturbances over the southern part of Japan are investigated. Figure 14 shows a forward trajectory starting at the same position and time with the backward trajectory shown above. It is found that the trajectory passed just near the JMA rawinsonde station, Ishigakijima, and that the air was transported in about 18 h from NongKhai to Ishigakijima. Figure 15 shows a time–height section of the meridional wind at Ishigakijima. The same filters used for the data at NongKhai were applied to the meridional wind shown in Fig. 15 in order to extract the same type of layered structures. In Fig. 15, layered disturbances with vertical scale of 2–4 km were observed at a height around 14 km during 17 and 21 January 2000. Figure 16 shows the vertical profiles of the meridional and zonal winds at Ishigakijima at 0000 UTC 20 January 2000, which is 18 h later than

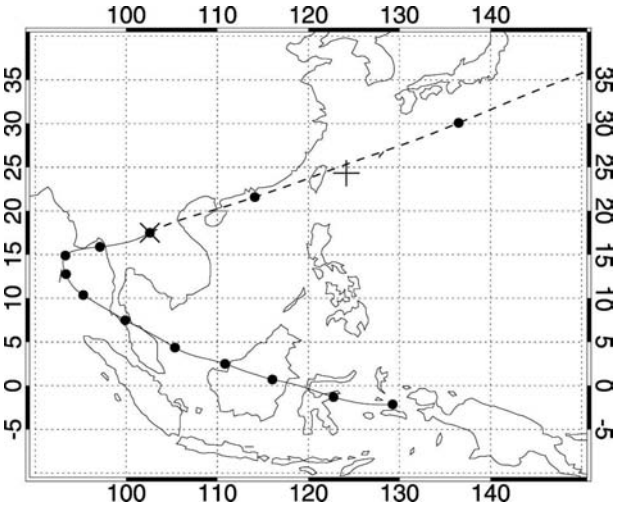

FIG. 14. Backward (solid line) and forward (dashed line) trajectories starting at NongKhai at 0600 UTC 19 Jan 2000. The distance between closed circles corresponds to 12 h.

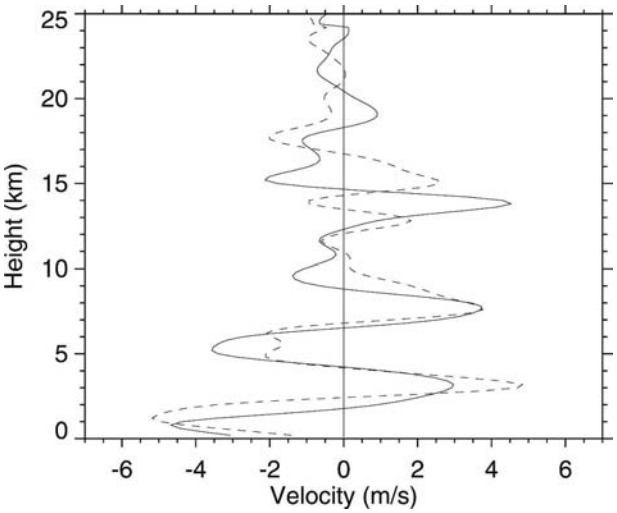

FIG. 16. As in Fig. 10 but for Ishigakijima at 0000 UTC 20 Jan 2000.

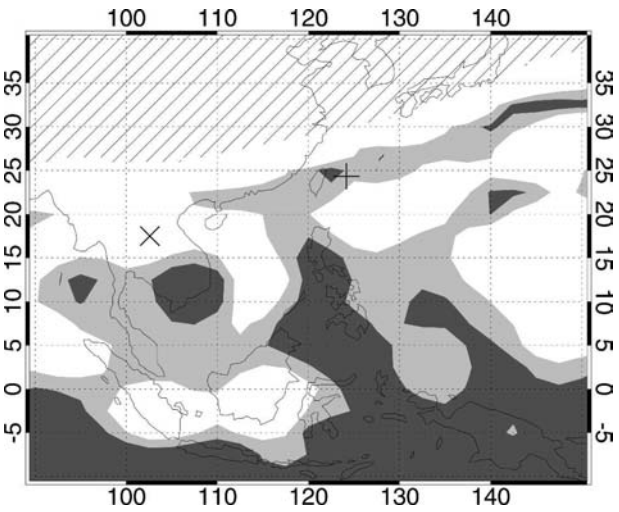

FIG. 17. As in Fig. 13 but for 0000 UTC 20 Jan 2000.

0600 UTC 19 January 2000. The phase relationship and amplitude ratio between the meridional and zonal winds are consistent with the disturbances due to inertial instability. The background PV was near zero, as shown in Fig. 17. Therefore, it can be concluded that both disturbances observed at NongKhai and Ishigakijima around 20 January 2000 were probably due to inertial instability embedded in the same air mass.

5. Summary

In this paper, we described the wave characteristics in the lower stratosphere over Thailand by utilizing the high-resolution rawinsonde data obtained by GAME-T enhanced observations. The frequency spectra, analyzed by taking advantage of the temporal high resolution of the data, showed three types of disturbances: 1) a 1-day wave at heights of 20–30 km, 2) a near-inertial period wave around 18 km, and 3) a layered disturbance with a period longer than 2.5 days at 12–17 km. The 1-day wave was considered to be the superposition of the migrating and nonmigrating tides. The near-inertial period wave was interpreted as a gravity wave propagating southwestward. The layered disturbances were inferred to be due to inertial instability, based on the fact that the meridional and zonal wind components had negative correlation and that the background atmosphere was near-inertially unstable.

The results shown in this paper are valuable and unique because disturbances with a vertical scale shorter than a few kilometers and temporal scale shorter then a few days over the Indochina Peninsula and the surrounding regions have not yet been examined by any past studies, mainly due to observation limitations. Similar observational studies are still expected in order to accumulate knowledge on the wave field over the region.

Acknowledgments. The enhanced observations were conducted with the cooperation of many GAME-related people. The authors thank Drs. M. E. Hagan and J. M. Forbes for providing their results of the GSWM and also for their helpful comments on the comparison between the model and observations of tidal waves in this paper. The comments on tidal waves by Drs. S. Miyahara and T. Nakamura were also helpful and encouraging.

REFERENCES

Allen, S. J., and R. A. Vincent, 1995: Gravity-wave activity in the lower atmosphere: Seasonal and latitudinal variations. *J. Geophys. Res.,* **100,** 1327–1350.

Eckermann, S. D., I. Hirota, and W. K. Hocking, 1995: Gravity wave and equatorial wave morphology of the stratosphere derived from long-term rocket soundings. *Quart. J. Roy. Meteor. Soc.,* **121,** 149–186.

Fetzer, E. J., and J. C. Gille, 1994: Gravity wave variance in LIMS temperatures. Part I: Variability and comparison with background winds. *J. Atmos. Sci.,* **51,** 2461–2483.

——, and ——, 1996: Gravity wave variance in LIMS temperatures. Part II: Comparison with the zonal-mean momentum balance. *J. Atmos. Sci.,* **53,** 398–410.

Fukao, S., T. Sato, N. Yamasaki, R. M. Happer, and S. Kato, 1980: Radar measurement of tidal winds at stratospheric heights over Arecibo. *J. Atmos. Sci.,* **37,** 2540–2544.

Hagan, M. E., M. D. Burrage, J. M. Forbes, J. Hackney, W. J. Randel, and X. Zhang, 1999: GSWM-98: Results for migrating solar tides. *J. Geophys. Res.,* **104,** 6813–6827.

Hirota, I., 1984: Climatology of gravity waves in the middle atmosphere. *J. Atmos. Terr. Phys.,* **46,** 767–773.

——, and T. Niki, 1985: A statistical study of inertia-gravity waves in the middle atmosphere. *J. Meteor. Soc. Japan,* **63,** 1055–1066.

Hitchman, M. H., and C. B. Leovy, 1985: Diurnal tide in the equatorial middle atmosphere as seen in LIMS temperatures. *J. Atmos. Sci.,* **42,** 557–561.

Kitamura, Y., and I. Hirota, 1989: Small-scale disturbances in the lower stratosphere revealed by daily rawinsonde observations. *J. Meteor. Soc. Japan,* **67,** 817–830.

Ogino, S.-Y., M. D. Yamanaka, and S. Fukao, 1995: Meridional variation of lower stratospheric gravity wave activity: A quick look at Hakuho-maru J-COARE cruise rawinsonde data. *J. Meteor. Soc. Japan,* **73,** 407–413.

——, ——, S. Kaneto, T. Yamanouchi, and S. Fukao, 1997: Meridional distribution of short-vertical-scale fluctuations in the lower stratosphere revealed by cross-equatorial ozonesonde observations on "Shirase." *Proc. NIPR Symp. Polar Meteor. Glaciol.,* **11,** 199–210.

——, ——, and S. Fukao, 1999a: Interannual and day-to-day variations of gravity wave activity in the lower stratosphere over eastern part of Japan observed in winter during 1989–95. *J. Meteor. Soc. Japan,* **77,** 413–429.

——, ——, Y. Shibagaki, T. Shimomai, and S. Fukao, 1999b: Horizontal variations of gravity wave activities in the lower strato-

sphere over Japan: A case study in the Baiu season 1991. *Earth Planets Space,* **51,** 107–113.

Sato, K., 1994: A statistical study of the structure, saturation and sources of inertio-gravity waves in the lower stratosphere observed with the MU radar. *J. Atmos. Terr. Phys.,* **56,** 755–774.

——, and T. J. Dunkerton, 2002: Layered structure associated with low potential vorticity near the tropopause seen in high-resolution radiosondes over Japan. *J. Atmos. Sci.,* **59,** 2782–2800.

——, T. Kumakura, and M. Takahashi, 1999: Gravity waves appearing in a high-resolution GCM simulation. *J. Atmos. Sci.,* **56,** 1005–1018.

——, M. Yamamori, S.-Y. Ogino, N. Takahashi, Y. Tomikawa, and T. Yamanouchi, 2003: A meridional scan of the stratospheric gravity wave field over the ocean in 2001 (MeSSO2001). *J. Geophys. Res.,* **108,** 4491, doi:10.1029/2002JD003219.

Shimizu, A., and T. Tsuda, 1997: Characteristics of Kelvin waves and gravity waves observed with radiosondes over Indonesia. *J. Geophys. Res.,* **102,** 26 159–26 171.

Tsuda, T., and S. Kato, 1989: Diurnal non-migrating tides excited by a differential heating due to land-sea distribution. *J. Meteor. Soc. Japan,* **67,** 43–55.

——, Y. Murayama, H. Wiryosumarto, S. W. B. Harijono, and S. Kato, 1994a: Radiosonde observations of equatorial atmosphere dynamics over Indonesia. 1. Equatorial waves and diurnal tides. *J. Geophys. Res.,* **99,** 10 491–10 505.

——, ——, ——, ——, and ——, 1994b: Radiosonde observations of equatorial atmosphere dynamics over Indonesia. 2. Characteristics of gravity waves. *J. Geophys. Res.,* **99,** 10 507–10 516.

——, M. Nishida, C. Rocken, and R. H. Ware, 2000: A global morphology of gravity wave activity in the stratosphere revealed by the GPS occultation data (GPS/MET). *J. Geophys. Res.,* **105,** 7257–7273.

Vincent, R. A., S. J. Allen, and S. D. Eckermann, 1997: Gravity-wave parameters in the lower stratospher. *Gravity Wave Processes and Their Parameterization in Global Climate Models,* K. Hamilton, Ed., Springer-Verlag, 7–25.

Wu, D. L., and J. W. Waters, 1996a: Gravity-wave-scale temperature fluctuations seen by the UARS MLS. *Geophys. Res. Lett.,* **23,** 3289–3292.

——, and ——, 1996b: Satellite observations of atmospheric variances: A possible indication of gravity waves. *Geophys. Res. Lett.,* **23,** 3631–3634.

Yamamori, M., and K. Sato, 2006: Characteristics of inertia gravity waves over the South Pacific as revealed by radiosonde observations. *J. Geophys. Res.,* **111,** D16110, doi:10.1029/2005JD006861.

Yamanaka, M. D., S. Ogino, S. Kondo, T. Shimomai, S. Fukao, Y. Shibagaki, Y. Maekawa, and I. Takayabu, 1996: Inertio-gravity waves and subtropical multiple tropopauses: Vertical wavenumber spectra of wind and temperature observed by the MU radar, radiosondes and operational rawinsonde network. *J. Atmos. Terr. Phys.,* **58,** 785–805.